DELPHI Collaboration

DELPHI 2002-061 CONF 595
28 June, 2002

Study of Tau-pairs Production in Untagged Photon-Photon Collisions at LEP2 and Measurement of Anomalous Magnetic and Electric Dipole Moments of the Tau Lepton

V.Zhuravlov
Joint Institute for Nuclear Research
Dubna, Russia

Abstract

Tau-pairs production in the process $e^+e^- \to e^+e^-\tau^+\tau^-$was studied using data collected by DELPHI experiment during 1997 – 2000 years. We have analysed untagged $\gamma\gamma$ collisions where both photons are quasi-real. The corresponding integrated luminosity is 650 pb^{-1}. The obtained values of the cross-section are found to be in a good agreement with QED prediction. In addition limits on anomalous magnetic and electric dipole moments of the tau lepton are determined. All presented results are preliminary.

Contributed Paper for ICHEP 2002 (Amsterdam)

1 Introduction

We present a study of untagged $e^+e^- \to e^+e^-\tau^+\tau^-$events collected by DELPHI detector in the period from 1997 to 2000 years at $\sqrt{s}$ between 183 and 208 GeV. The total integrated luminosity used in the analysis is 650 pb^{-1}.

The final state $ee\tau\tau$ can be produced by bremsstrahlung of a single virtual photon in t-channel and s-channel, by conversion and by collision of two virtual photons – contribution of so-called multiperipheral graph. For untagged events with both electron and positron scattered by the small angle and not observed in the detector the dominant process is virtual photon collision (Fig 1). This process has been studied at LEP by L3 collaboration [1] and has been observed by OPAL collaboration [2].

The study of the reaction $e^+e^- \to e^+e^-\tau^+\tau^-$explores two fundamental problems. First of all it provides a deep test of QED at the level of forth order of α. Furthermore, the $\gamma\tau\tau$ vertex is sensitive to anomalous electromagnetic couplings of the tau lepton. Tree-level diagram of the $e^+e^- \to e^+e^-\tau^+\tau^-$process consist of two of such vertexes, therefore anomalous magnetic and electric dipole moments can be extracted from comparison of the measured cross-section with QED expectation.

This note gives detailed description of tau-pairs selection, background estimation, selection and trigger efficiency calculation as well as systematic errors estimation. We also describe the computation of the anomalous electromagnetic moments of the tau lepton.

2 Monte-Carlo simulation

To simulate the signal process we used generator of Berends, Daverveldt and Kleiss RADCOR (BDKRC) [3] which calculates the cross-section of multipheriferal diagram with the radiative corrections on the electron and positron lines. Only untagged $e^+e^- \to e^+e^-\tau^+\tau^-$events were generated with BDKRC which makes accepted cross-section 1.5 % less than total. The τ decay is simulated by TAUOLA package [5] which includes photon radiation from the decay products. BDKRC generator was also used to estimate the background coming from the process $e^+e^- \to e^+e^-\mu^+\mu^-$. To simulate $e^+e^- \to e^+e^-e^+e^-$ background we used generator of Berends, Daverveldt and Kleiss DIAG36 (BDK) [4]. This generator takes into account multiperipheral diagram and also all possible non-multiperipheral diagrams and their interference to multiperipheral diagram. Hadron production in two photon collisions was simulated by PYTHIA 6.1 generator [6]. WW and ZZ events were simulated by WPHACT generator [11]. Contribution from tagged $e^+e^- \to e^+e^-\tau^+\tau^-$events (considered as a background) was also simulated by WPHACT.

The generated events were passed through the full simulation program of the DELPHI detector [7] and were reconstructed with the same program [8] as for the real data.

3 Event selection

In an untagged event both electron and positron scatter at small angles and remain undetectable escaping to the beam pipe. Therefore only decay products of the tau leptons can be seen in the detector. To suppress background we consider only one-prong decay

channels with one tau decaying into electron and the other into non-electron (hadron or muon).

The track selection and event analysis was performed with the aid of TAUPLUS package [9]. To select runs with good performance of the sub-detectors [10] we retained runs with Time Projection Camber (TPC) and electromagnetic calorimeters (HPC and FEMC) nominally operational. Also we required one of the the Forward Chambers (FCA, FCB) and one of the additional barrel tracking detectors (ID or VD) to be nominally operational.

For the period of failure of TCP sector 6 in year 2000 the run quality criterion for the corresponding half of the TPC was released.

The event selection procedure was divided into two steps. At the first step (preselection) we selected the sample of two good track events with non-zero accoplanarity The definition of the good track is the following:

- track length more than 30 cm
- track momentum more than 100 MeV
- momentum resolution less than 100 %
- the distance of closest approach of the track to the beam spot along z-axis [1] less then 10 cm, the distance in $r - \phi$ plane less then 5 cm
- the distance from the beam spot to the the first measured point on the track less then 25 cm
- the polar angle of the track θ between 20° and 160°

The following set of cuts were applied at the first step of selection:

- We required exactly two good tracks with opposite charges and at least one of the tracks should have momentum greater than 300 MeV.
- To suppress background from fermion pairs production total kinetic energy of the charged particles should be less then 30 GeV.
- In order to enrich the sample with $e^+e^- \to e^+e^-\tau^+\tau^-$events we required the accoplanarity [2] to be greater than 0.5° and the transverse momenta calculated both for two tracks and for all particle visible in the detector to be greater than 500 MeV. Transverse momentum defined as radial component of vector sum of momenta.
- To select the events with high trigger efficiency we required the transverse energy to be greater than 2 GeV. Transverse energy defined by

$$E_t = p_1 \sin\theta_1 + p_2 \sin\theta_2,$$

where p_1 and p_2 are absolute values of momenta of particles and θ_1 and θ_2 are their polar angles.

[1] The DELPHI coordinate system has the z-axis aligned along the electron beam direction, the x-axis points toward the center of LEP and the y-axis is vertical. r is used to measure the radius in the (x,y) plane. The polar angle θ is measured with respect to the z-axis and the azimuthal angle ϕ is about z.

[2] Accoplanarity is defined as $180° - |\phi_2 - phi_1|$.

- Events with at least one track in sector 6 of the TPC were rejected for year 2000 because dE/dx measurement vital for this analysis was poor during the whole year.

- Finally, single and double tagged events were rejected by requiring that no energy deposition in STIC or FEMC exceeded 60% of the beam energy.

After applying of all the cuts described above the event composition in the preselected sample was found to be as follows (1999 year):

$$\begin{array}{ll} e^+e^- \to e^+e^-e^+e^- & 41\ \% \\ e^+e^- \to e^+e^-\mu^+\mu^- & 47\ \% \\ e^+e^- \to e^+e^-\tau^+\tau^- & 8\ \% \\ e^+e^- \to e^+e^-q\bar{q} & 3\ \% \\ e^+e^- \to \tau^+\tau^- & 1\ \% \end{array}$$

Fraction of other events was less than 1%.

Figure 2 shows the comparison between data and Monte-Carlo after the first step of selection for 1999 year. The distributions of visible invariant mass, charged energy as well as transverse energy and transverse momentum of two charge particles are presented. Distribution of $e^+e^- \to e^+e^-\tau^+\tau^-$events is shown with dashed histogram. Monte-Carlo was normalised to the luminosity of the data and was not corrected for trigger efficiency.

At the final step of selection the dE/dx pull for muon, electron, kaon and proton hypotheses is widely used. The dE/dx pull for specific particle hypothesis is defined as a ratio

$$\Pi = \frac{(dE/dx)_{meas} - (dE/dx)_{exp}}{\sigma_{dE/dx}},$$

where $(dE/dx)_{exp}$ is value expected for the particle with given momentum. The calibration of the dE/dx on the DST level is not perfect and dE/dx pull has a strong dependence on azimuthal and polar angle and essential disagreement between data and Monte-Carlo. The following calibration procedure was developed to correct this effect. From preselected events the sample of $e^+e^- \to e^+e^-\mu^+\mu^-$ events was selected by requirement of dE/dx pull for electron hypothesis $\Pi_e < -3.2$ for one track. The distributions of the muon pull of the other track were used to determine its dependence on azimuthal and polar angles. Then the corresponding function of azimuthal and polar angle were added to the values of the muon pull to diminish the angular dependence. The same procedure was performed with simulated $e^+e^- \to e^+e^-\mu^+\mu^-$ events and real and simulated distributions of the corrected muon pull were compared. Residual disagreement was removed by scaling and smearing of the muon pull in simulated events. Similar algorithm was applied to correct the electron pull. From the corrected muon and electron pulls the corrected dE/dx was calculated by the formula

$$dE/dx = \frac{(dE/dx)_e\Pi_\mu + (dE/dx)_\mu\Pi_e}{\Pi_\mu + \Pi_e}$$

and proton and kaon pulls were recalculated with corrected value of dE/dx. Independent calibration to real and simulated data for each analysed year of data taking was performed.

With corrected dE/dx information we identified a track as an electron if $\Pi_\mu > 3.2$ while for non-electron candidate we required $\Pi_e < -3.2$. The event was retained if one of the its tracks was identified as electron and the other was identified as non-electron. Fig. 3 illustrates the particle identification cuts. The distributions of electron and muon

pull hypotheses are shown for 1999 year real data and simulation. For each distribution all other cuts are applied besides the cut on the shown variable. Dashed histograms are signal.

A considerable amount of kaon and proton background from $\gamma\gamma \to q\bar{q}$ events remained after cuts on pulls for muon and electron hypotheses. Fig. 4 (left) shows specific energy loss for electron candidate plotted versus momentum of the particle. Proton and kaon bands are clearly visible. To remove kaon and proton background additional cuts were applied. The dE/dx for the electron candidate should not be grater then 1.9 in units of M.I.P. and pulls for proton and kaon hypotheses for the electron candidate both should be out of $\pm 1.5\sigma$ interval: $|\Pi_K| > 1.5$ and $|\Pi_P| > 1.5$. Fig.4 (right) shows the distribution of the pull for proton hypothesis with all selection cuts applied except the cut on shown variable. Black histogram shows the background from $e^+e^- \to q\bar{q}$ events and dashed histogram show the rest of background. The cuts on this variable are indicated by arrows.

4 Trigger efficiency

Low momenta of the tracks in the process $e^+e^- \to e^+e^-\tau^+\tau^-$with untagged electron and positron and requirement of only two tracks in event make the probability to trigger such event essentially below 100%. Therefore the determination of the trigger efficiency is important in this analysis.

We estimated trigger efficiency from the selected events exploring the fact that an event can be detected by different components of DELPHI trigger system. From all selected events we picked out those with one track directed into barrel and the other directed into end-cup using the following definition:

$$\begin{array}{ll} \text{Barrel track:} & 45^\circ < \theta < 135^\circ \\ \text{End-cup track:} & \theta < 35^\circ \text{ or } \theta > 145^\circ. \end{array}$$

Trigger subcomponents were combined into barrel and end-cup triggers. Barrel trigger was combined by "OR" of ID*OD*[HAB+MUB], TPC Barrel+IDOD6 and "Single gamma barrel". End-cup trigger consists of "OR" of "Single forward", "Single gamma forward", "Single backward" and "Single gamma backward". Number of events detected by barrel trigger (N_B), number of events detected by end-cup trigger (N_E) and number of events detected by both barrel and end-cup trigger (N_{BE}) were counted using decision functions of the third-level trigger. Barrel and end-cup trigger efficiencies to single track were calculated by the formulae:

$$\varepsilon_{Barrel} = \frac{N_{BE}}{N_E}$$

$$\varepsilon_{End-Cup} = \frac{N_{BE}}{N_B}$$

Results of trigger efficiency calculation are summarised in Table 1.

5 Efficiency of dE/dx measurement

Both tracks of the selected event should have specific energy loss measurement. An imperfect detector simulation can lead to discrepancy in efficiency of dE/dx measurement

	1997	1998	1999	2000
Singe barrel, %	80.0 ± 6.0	89.1 ± 2.7	82.9 ± 2.8	78.9 ± 3.8
Single end-cup, %	22.2 ± 6.2	34.5 ± 4.1	23.4 ± 3.2	18.8 ± 3.0
Tau pair, %	85.6 ± 4.9	92.9 ± 2.1	88.1 ± 2.3	83.4 ± 3.1

Table 1: Summary of the trigger efficiency measurement

for the good track in real and simulated events. To take into account possible disagreement we calculate the efficiency of the good track to have dE/dx measurement (to be "good TPC track") for the muon pairs sample extracted from preselected events. Muon events were selected be requirement that at least one track was identified by muon chamber. For these events the efficiency of "good TPC track" was determined as the ratio

$$\varepsilon_{dE/dx} = \frac{N_{dE/dx}}{N_{tot}}$$

where $N_{dE/dx}$ is number of events with both track having dE/dx measurement and N_{tot} is the total number of selected muon pairs. Efficiencies for "good TPC track" computed for data and $e^+e^- \to \mu^+\mu^-$ Monte-Carlo are presented in Table 2. Good agreement between simulated and real events was found. The calculated values were used for selection efficiency correction and for systematic errors estimation. The selection efficiency was multiplied by factor $\frac{\varepsilon_{dE/dx}(data)}{\varepsilon_{dE/dx}(MC)}$ and half of the difference was included into systematic error together with uncertainties from the test sample statistics.

	1997	1998	1999	2000
Efficiency in data, %	80.6 ± 0.5	80.6 ± 0.3	80.4 ± 0.3	80.6 ± 0.3
Efficiency in MC, %	79.6 ± 0.1	79.8 ± 0.1	79.7 ± 0.1	80.0 ± 0.1

Table 2: Summary of "good TPC track" efficiencies estimation

6 Background

We have considered several sources of background for $e^+e^- \to e^+e^-\tau^+\tau^-$events:

- The background from $e^+e^- \to e^+e^-q\bar{q}$, mainly proton and kaon production due to the tails of dE/dx pulls for proton and kaon hypotheses.
- The background from $e^+e^- \to e^+e^-e^+e^-$ events due to the tail of the distribution of the dE/dx pull for muon hypothesis.
- Similar background from $e^+e^- \to e^+e^-\mu^+\mu^-$ events.
- The process $e^+e^- \to \tau^+\tau^-$.
- Background due to WW and ZZ production
- Tagged $e^+e^- \to e^+e^-\tau^+\tau^-$events

- Background from fermion pairs production other than tau pairs was found to be negligible.

Background fractions for main background sources are summarised in Table 3.

Channel	97	98	99	2000
$ee \to \tau\tau$	1.26 ± 0.03	1.81 ± 0.05	0.30 ± 0.01	0.27 ± 0.01
$ee \to eeee$	1.4 ± 0.2	2.3 ± 0.1	1.9 ± 0.1	0.8 ± 0.1
$ee \to ee\mu\mu$	2.9 ± 0.1	3.7 ± 0.1	1.4 ± 0.1	1.6 ± 0.1
$ee \to eeq\bar{q}$	4.5 ± 1.5	3.3 ± 0.7	3.5 ± 0.8	3.2 ± 0.8
$ee \to WW$, ZZ and tagged $e^+e^- \to e^+e^-\tau^+\tau^-$	1.5 ± 0.3	1.4 ± 0.3	1.2 ± 0.3	1.1 ± 0.2
Total	11.5 ± 1.5	12.5 ± 0.8	8.4 ± 0.9	6.9 ± 0.8

Table 3: Summary of background fractions. The numbers are the expected fractions (%) of specified background in selected sample. Errors are statistical errors of simulated samples and theoretical uncertainties of the Monte-Carlo generators added in quadratures.

7 Systematic errors estimation

The following sources of systematic error were considered: uncertainties of selection and trigger efficiencies and uncertainty of background level. Track selection, event selection and statistical error of simulated samples were taken into account for the calculation of selection efficiency uncertainty.

The systematic error arising from track selection was estimated in the following way. Each cut of the track selection was varied from its nominal value in both directions typically by 10%. The corresponding change of the cross-section Δ was compared to the value of the expected statistical fluctuation σ which arises from non-identical event sample. If the value Δ was less then σ no systematic error was ascribed to the corresponding cut, in the opposite case the value of $\sqrt{\Delta^2 - \sigma^2}$ was included into systematic error. The systematic error arising from variation of event selection cuts was estimated in a similar way.

Uncertainties of the determination of angular correction applied to dE/dx pulls hypotheses for muon and electron were used to calculate the systematic error caused by dE/dx corrections. The correction functions were varied by the uncertainty of each of their parameters and the analysis chain was repeated. The variation of the measured cross-section was added to the systematic error. Similarly the systematic error corresponding to pulls scaling and smearing were calculated. The summary of the systematic errors associated with track selection cuts, events selection cuts and dE/dx correction are presented in Table 4. The numbers are given for 1999 year, for other years the values are similar.

Additional contribution to the systematic error also presented in Table 4 gives the statistical error of Monte-Carlo sample and the correction of selection efficiency which described in section 5.

The main contribution to the systematic error gives the uncertainty of the trigger efficiency dominated by statistics of data events, see chapter 4 and Table 1.

syst.source		value, %
track selection cuts		
	R_{imp}	0.7
	Z_{imp}	1.1
	$\delta p/p$	0.7
event selection cuts		
	Π_e	0.3
	Π_μ	0.3
	accoplanarity	0.6
dE/dx corrections		
	Π_e θ	1.0
	Π_e ϕ	0.9
	Π_μ θ	1.0
	Π_μ ϕ	1.0
	scaling	0.7
	smearing	0.6
MC statistics		0.8
"Good TPC track" correction		0.5
Total		2.9

Table 4: Systematic errors coming from track selection, event selection, dE/dx corrections, simulated samples statistics and "good TPC track" correction.

The systematic error due to residual background includes the simulated sample statistical uncertainty and theoretical uncertainty of Monte-Carlo generators mainly for $ee \to eeq\bar{q}$ process.

The systematic errors from trigger efficiency, selection efficiency and residual background are summarised in Table 5. The sources of selection efficiency uncertainty are described in details in Table 4. Total systematic errors calculated as sum in quadrature of all described components are also presented in Table 5.

	1997	1998	1999	2000
Trigger eff.%	5.7	2.3	2.6	3.7
Selection eff.%	4.9	3.2	2.9	2.8
Background %	1.7	0.9	1.0	0.9
Total %	7.7	4.0	4.0	4.8

Table 5: Systematics errors coming from trigger efficiency, selection efficiency and residual background and total systematic errors.

8 Results of the cross-section measurement

The numbers of observed and predicted events, their ratios together with values of selection efficiency are presented in Table 6. Expected numbers of events are corrected for trigger efficiency and selection efficiency was calculated from $e^+e^- \to e^+e^-\tau^+\tau^-$Monte-Carlo sample and corrected as described in section 5.

Year	Observed	Predicted	Obs./Pred.	Sel. eff, %
1997	203	193 ± 11	1.05 ± 0.10	0.90
1998	581	599 ± 14	0.97 ± 0.05	0.86
1999	815	785 ± 22	1.04 ± 0.05	0.81
2000	555	513 ± 20	1.08 ± 0.06	0.57

Table 6: The numbers of observed and expected events, ratios of observed and expected events and selection efficiencies

The cross-sections were computed using the formula

$$\sigma = \frac{N_{obs} - N_{bg}}{\varepsilon_{sel}\varepsilon_{trig}\mathcal{L}}$$

where N_{obs} is number of observed events, N_{bg} is expected number of background events, ε_{sel} is selection efficiency, ε_{trig} is trigger efficiency and $\mathcal{L}$ is integrated luminosity.

The measured cross-section are compared to the prediction of BDKRC Monte-Carlo simulation in Table 7. Agreement between data and QED prediction was found.

Year	σ_{MC}, pb	σ_{meas}, pb
1997	428.2 ± 0.5	$439.2 \pm 35.3 \pm 33.8$
1998	436.7 ± 0.5	$412.6 \pm 19.9 \pm 16.5$
1999	448.5 ± 0.5	$460.7 \pm 17.8 \pm 18.4$
2000	459.4 ± 0.5	$487.1 \pm 21.8 \pm 23.4$

Table 7: The measured cross-sections and QED predictions. First error on measured cross-sections is statistical error, the second one is systematic error.

In fig. 5 we compare the distributions of electron and non-electron candidate momenta to the Monte-Carlo prediction for combined 1997-2000 years data. Fig 6 shows the invariant mass distribution for selected events also for combined 1997-2000 years. Trigger efficiency is taken into account in these distributions.

9 Determination of anomalous magnetic and electric dipole moments

In Standard Model (SM) leptons are considered as a point-like objects, thus the observation of a deviation of magnetic and electric dipole moments of the leptons from their SM values would make a window to the physics beyond SM. The anomalous magnetic

moments of the electron [12] and muon [13] are known with superior precision while the short life-time of the tau-lepton does not allowed to measure the anomalous moments with similar precision by a spin precession method.

The generalised form of the $\tau\tau\gamma$ vertex can be parametrise in the following form:

$$-ie\bar{u}(p')(F_1(q^2)\gamma_\mu + iF_2(q^2)\sigma_{\mu\nu}\frac{q_\nu}{2m_\tau} + F_3(q^2)\gamma^5\sigma^{\mu\nu}\frac{q_\nu}{2m_\tau})u(p)\epsilon_\mu(q)$$

where ϵ_μ is the poliarization vector of the photon with momentum q. Form factor F_1 describes the distribution of electric charge and $e_\tau = F_1(0)$, while F_2 and F_3 are form factors related to the magnetic moment a_τ and electric dipole moment d_τ:

$$a_\tau \equiv \frac{g_\tau - 2}{2} = F_2(0)$$

and

$$F_3(0) = \frac{d_\tau}{e_\tau}$$

In SM at tree level $a_\tau = 0$ and $d_\tau = 0$. Accounting of loop diagrams gives a non-zero value to $a_\tau = 11773(3) \cdot 10^{-7}$ [14], while non-zero value of d_τ violate CP invariance.

The values of a_τ and d_τ have been measured by several groups. L3 and OPAL collaborations [15, 16] studied the radiative $Z \to \tau\tau\gamma$ events and set the 95 % CL limits on the values of anomalous magnetic and electric dipole moments:

$$\begin{array}{lll} -0.052 < a_\tau < 0.058 & \text{and } |d_\tau| < 3.1 \cdot 10^{-16}\ e \cdot cm & \text{(L3)} \\ -0.068 < a_\tau < 0.065 & \text{and } |d_\tau| < 3.7 \cdot 10^{-16}\ e \cdot cm & \text{(OPAL).} \end{array}$$

Using the combination of LEP1, LEP2 and SLD data on $e^+e^- \to \tau^+\tau^-$ production cross-section the 2σ limit of

$$-0.007 < a_\tau < 0.005$$

has been set by [17]. Another limit can be found in [18] obtained from data of $e^+e^- \to \tau^+\tau^-$ production at LEP:

$$\begin{array}{l} -0.004 < a_\tau < 0.006 \\ |d_\tau| < 1.1 \cdot 10^{-17}\ e \cdot cm. \end{array}$$

In [19, 20] the limits of

$$\begin{array}{l} |F_2| < 0.014 \\ |F_3| < 0.025 \end{array}$$

are obtained from $e^+e^- \to \tau^+\tau^-$ process at PETRA. However these limits cat not be directly translated into the limits on a_τ and d_τ because the limits were derived from cross-section of q^2 up to (37 GeV)^2.

Using the ARGUS detector at e^+e^- storage ring DORIS II the search for the real and imaginary part of the electric dipole form factor of the tau lepton was performed [21]. The following results were derived from the production of tau pairs at $q^2 = 100\ GeV^2$:

$$\begin{array}{ll} \Re e(d_\tau) & = (1.6 \pm 1.9) \cdot 10^{-16}\ e \cdot cm \\ \Im m(d_\tau) & = (-0.2 \pm 0.8) \cdot 10^{-16}\ e \cdot cm \end{array}$$

Here we present the study of anomalous magnetic and electric dipole moments of the tau lepton based on the analysis of cross-section of $e^+e^- \to e^+e^-\tau^+\tau^-$process. The kinematic region of the two-photon processes is complimentary to the one in the processes mediated by Z and γ, where the bounds described above have been obtained. The study of anomalous coupling of tau lepton to photon at LEP was proposed in [22]

To model the contribution of non-SM anomalous magnetic and dipole moments we use the calculation by Cornet [23]. The calculation is based on computation of the matrix element of the process $\gamma\gamma \to \tau\tau$ in leading order of QED and its translation to the cross-section of $e^+e^- \to e^+e^-\tau^+\tau^-$process using Equivalent Photon Approximation (EPA) [24]. To tune the quantity of $(-q^2)_{max}$ used in EPA (upper limit of the integration over 4-momenta of emitted photon) we compare the result of BDKRC calculation with non-SM calculation with anomalous moments set to their SM values. The best agreement was achieved with $(-q^2)_{max} = 0.366(\mathrm{GeV})^2$.

Figure 7 shows the total cross-section change as a function of anomalous magnetic moment and as a function of electric dipole moment. Three lines on each plot represent calculation with $\sqrt{s}$ =182.7, 195.5 and 205.0 GeV. Increase of collision energy slowly give rise to both non-SM contributions, however anomalous magnetic moment can either increase or decrease the cross-section while the electric dipole moment tends only to increase the cross-section.

To compare experimentally measured values of the cross-sections to non-SM calculation we convert them from untagged events cross-sections into total cross-sections. Conversion factors were calculated by means of BDKRC generator and yielded to 1.5% difference. The validity of the applying of SM conversion factors is supported by the fact that measured cross-sections are in a good agreement with SM prediction what guarantees the smallness of the non-SM contribution, and from the other hand, the correction itself is small enough.

Fit of the cross-sections measured at 1997, 1998, 1999 and 2000 years of data taking for the parameters of a_τ and d_τ was performed. When fitting for a_τ we set the value of d_τ to its SM value and *vice versa*. As an error of the cross section measurement we took statistical and systematic errors added in quadrature.

To quote the obtained limits we used the following convention:

$$\int_{-\infty}^{L} \exp\left(-\chi^2\right) da_\tau = \int_{R}^{\infty} \exp\left(-\chi^2\right) da_\tau = \frac{1-CL}{2}$$

where χ^2 is the χ^2-function, CL is desired confidence level, L and R are lower and upper limits. Similar definition used for d_τ We quote central value μ and error σ for moments according to

$$\sigma = \frac{R-L}{2}, \mu = \frac{R+L}{2}.$$

where R and L are calculated with 68.3 % confidence level.

Fig. 8 shows the χ^2 as a function of anomalous magnetic moment and as a function of electric dipole moment. The results of the fit are:

$$\begin{array}{ll} -0.017 < a_\tau < 0.019, & 95\%\ \mathrm{CL} \\ |d_\tau| < 3.8 \cdot 10^{-16}\ e \cdot cm, & 95\%\ \mathrm{CL}. \end{array}$$

Figure 9 shows the difference between measured cross-section and SM expectation as a function of $\sqrt{s}$. Two lines superimposed to the plot represent the cross-section calculation

with upper limit of $a_\tau = 0.019$ and upper limit of $d_\tau = 3.8 \cdot 10^{-16}\ e \cdot cm$. The results expressed in the form of central value and error calculated with above formulae with 68.3 % confidence level are as following:

$$a_\tau = 0.003 \pm 0.009,$$
$$d_\tau = (0.0 \pm 2.4) \cdot 10^{-16}\ e \cdot cm.$$

10 Conclusion

We have studied the reaction $e^+e^- \to e^+e^-\tau^+\tau^-$in untagged topology with the data collected with the DELPHI detector during LEP operation in 1997-2000 years. Obtained values of cross-section agree with QED expectation. The measured cross-sections were used to extract the limits on anomalous magnetic and electric dipole moments of the tau lepton. The obtained 95% CL limits are

$$-0.017 < a_\tau < 0.019$$
$$|d_\tau| < 3.8 \cdot 10^{-16}\ e \cdot cm.$$

11 Acknowledgements

We thank to F.Cornet, who provide the calculation of the cross-section of the anomalous tau-pairs production in two-photon collisions.

References

[1] L3 collaboration., M. Acciarri *et al.* , Phys. Lett. **B407** (1997) 341.

[2] OPAL Collaboration, R. Akers *et al.* , Zeit. fur Physik **C60** (1993) 593.

[3] F.A. Berends, P.H. Daverveldt, R. Kleiss Comp. Phys. Comm., **40** (1986) 271.

[4] F.A. Berends, P.H. Daverveldt, R. Kleiss Comp. Phys. Comm., **40** (1986) 285.

[5] S. Jadach, J. Kühn, Z. Wąs Comp. Phys. Comm., **64** (1991) 275.

[6] T. Sjostrand, S. Mrenna, PYTHIA 6.2: PHYSICS AND MANUAL, hep-ph/0108264

[7] DELPHI Collaboration, *DELSIM Delphi event Generator and Detector Simulation User's Guide*, DELPHI/89-67 (1989)

[8] DELPHI Collaboration, *DELPHI Data Analysis Program (DELANA) User's Guide*, DELPHI/89-44 (1989)

[9] S. de Brabandere, M.Dam and D.Edsall, *TAUPLUS, A Tau Physics Analysis Package*, DELPHI/94-131 (1994)

[10] Detailed description of DELPHI subdetectors can be found in:
DELPHI collaboration, Nucl.Instr. and Meth **A303** (1991) 233. DELPHI collaboration, Nucl.Instr. and Meth **A378** (1996) 57.

[11] E.Accomando, A. Ballestrero, *WPHACT 1.0, A program for WW, Higgs and 4 fermion physics at e^+e^- colliders*, DFTT 16/96 (1996)

[12] P.J. Mohr, B.N. Taylor, J. Phys. Chem. Ref. Data **28**, (1999) 1713;
P.J. Mohr, B.N. Taylor, Rev. Mod. Phys. **72**, (2000) 351.

[13] D.W. Hertzog, hep-ex/0202024 (2002).

[14] M.A. Samuel, G. Li, R.Mendel, Phys. Rev. Lett. **v67**, 6, (1991) 668.

[15] L3 Collaboration, M. Acciarri *et al.* , Phys. Lett. **B438**, (1998), 169.

[16] OPAL Collaboration, K.Ackerstaff *et al.* , Phys. Lett. **B431**, (1998),188.

[17] G.A. Gonzalez, A. Santamaria and J.Vidal, Nucl. Phys **B582**, (2000), 3.

[18] R. Escribano, E.Massó, Phys. Lett., **B395**, (1997), 369.

[19] D.J. Sivarman, G.L.Shaw, Phys. Rev. **D27**, (1983), 1196.

[20] F. del Aguila, M.Sher, Phys. Lett, **B252**, (1990), 116

[21] ARGUS Collaboration, H.Albrecht *et al.* , Phys. Lett. **B485**, (2000), 37

[22] F. Cornet and J.Illana, Phys. Rev **53**, 3, (1996), 1181

[23] F. Cornet, private communication.

[24] V.M. Budnev *et al.* , Phys. Rep. **15C**, (1975), 181

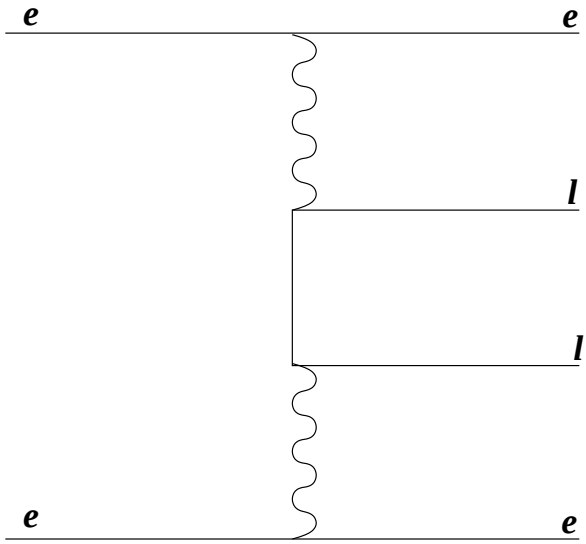

Figure 1: The dominant diagram for the reaction $e^+e^- \to e^+e^-\tau^+\tau^-$

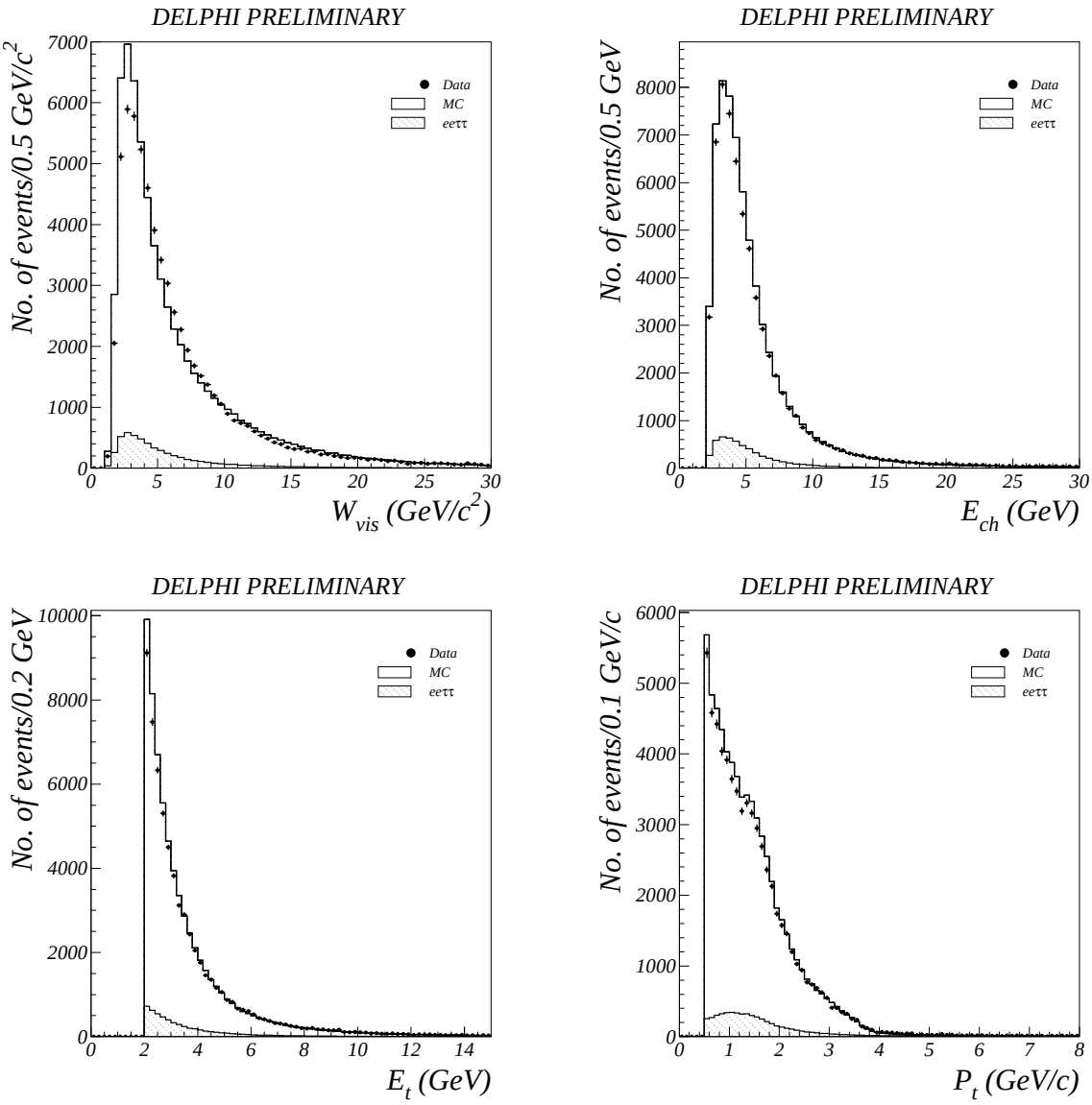

Figure 2: The distributions of visible invariant mass, charged energy, transverse energy and transverse momentum of two charged particles. Preselection cuts are applied.

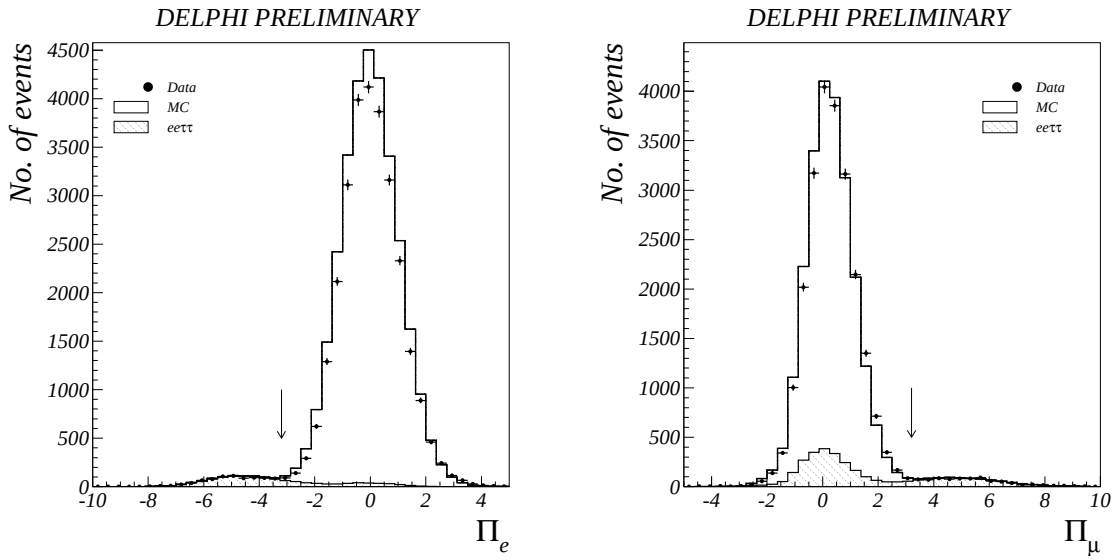

Figure 3: Distribution of dE/dX pull for electron hypothesis and distribution of dE/dX pull for muon hypothesis with all selection cuts are applied except the cut on the variable shown.

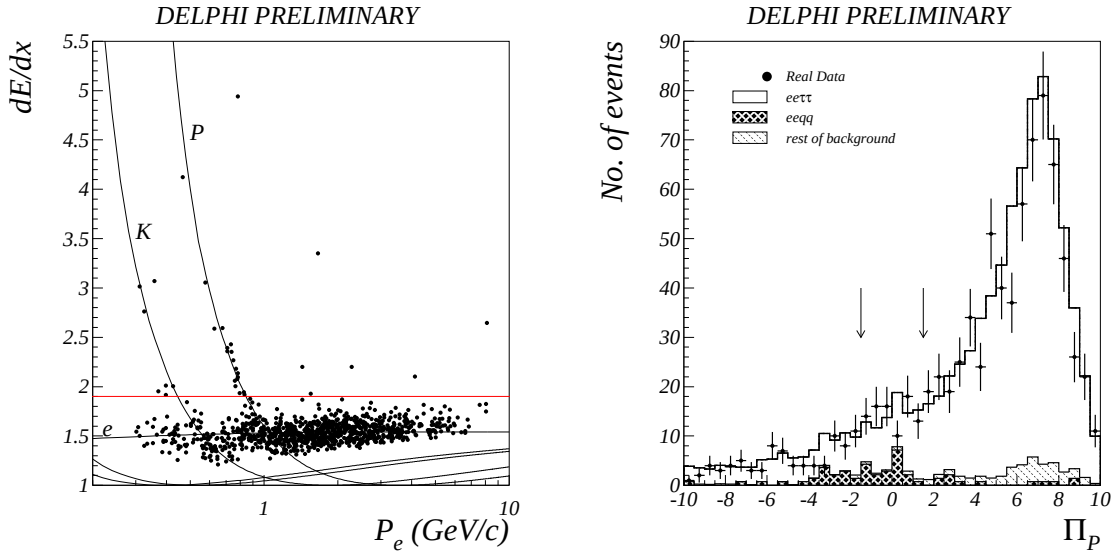

Figure 4: Left: specific energy loss for electron candidate after cuts on electron and muon pulls as a function of particle's momentum. Right: distribution of dE/dx pull for proton hypothesis for electron candidate. Black histogram is the background from $e^+e^- \to q\bar{q}$ events and dashed histogram is the rest of background. The cuts on this variable are indicated by arrows. All other selection cuts are applied.

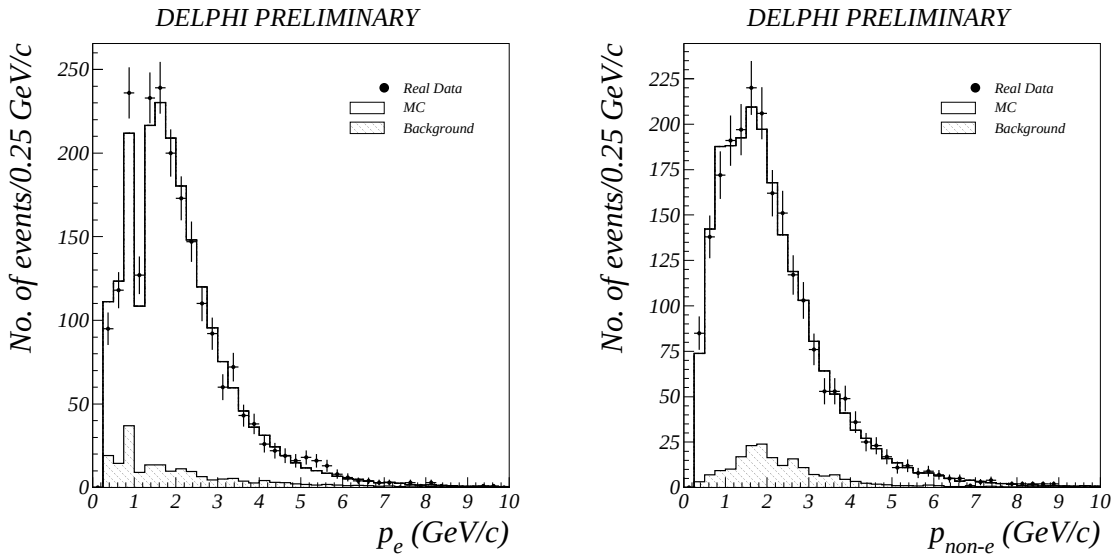

Figure 5: Momentum distribution for electron candidate and non-electron candidate for combined 1997-2000 years. Monte-Carlo is corrected for trigger efficiency.

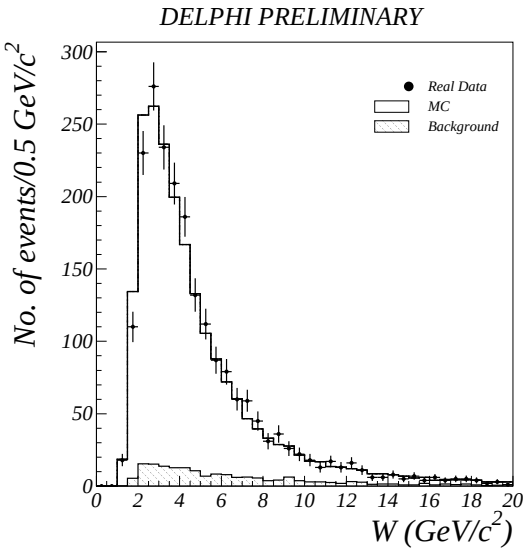

Figure 6: Invariant mass distribution for selected events for combined 1997-2000 years. Monte-Carlo is corrected for trigger efficiency.

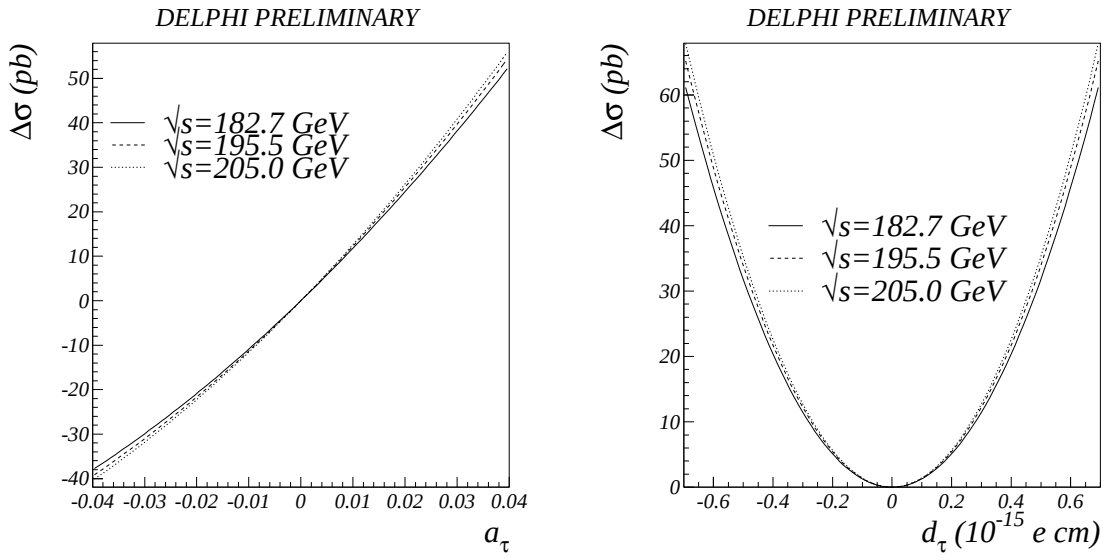

Figure 7: Total cross-section change as a function of anomalous magnetic moment and as a function of electric dipole moment.

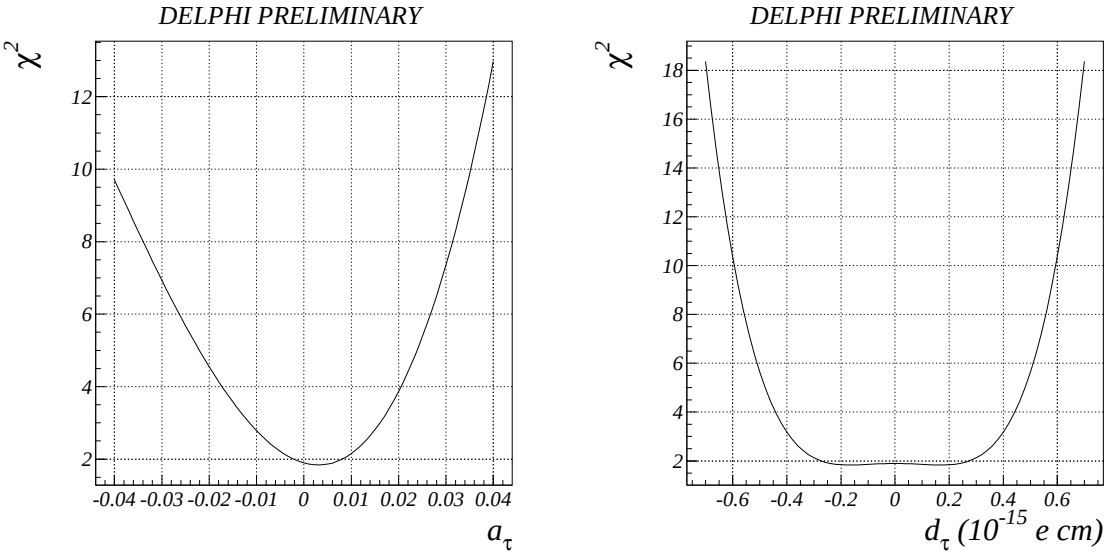

Figure 8: χ^2 as a function of anomalous magnetic moment and as a function of electric dipole moment

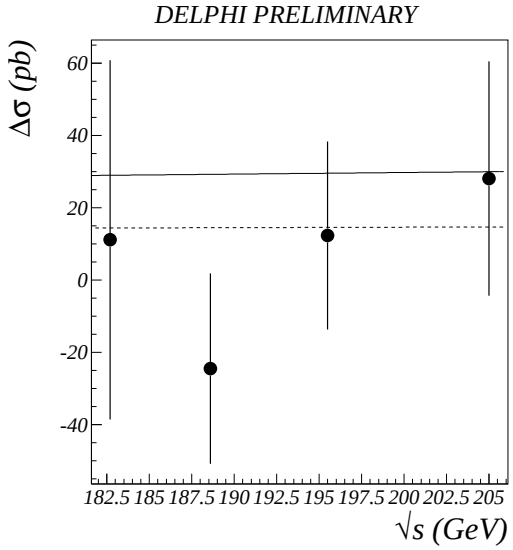

Figure 9: Difference between measured cross-section and SM expectation as a function of $\sqrt{s}$. Superimposed lines are the results of non-SM calculation with our upper limits on anomalous moments: $a_\tau = 0.019$ (solid line) and $d_\tau = 3.8 \cdot 10^{-16}\ e \cdot cm$ (dashed line).